Design and Test of Three Active Flutter Suppression Controllers

David M. Christhilf
Lockheed Engr. and Sc. Co.
144 Research Drive
Hampton, VA 23666
(804) 864-4029

William M. Adams
Mail Stop 489
NASA Langley Research Center
Hampton, VA 23665
(804) 864-4013

Martin R. Waszak
Mail Stop 489
NASA Langley Research Center
Hampton, VA 23665
(804) 864-4015

Dr. S. Srinathkumar
National Research Council Associate
Bangalore 560 017
India

Dr. Vivek Mukhopadhyay
Mail Stop 243
NASA Langley Research Center
Hampton, VA 23665
(804) 864-2835

Presented at the
Fourth Workshop on Computational Control
of Flexible Aerospace Systems
Williamsburg, Virginia
July 11-13, 1990

ABSTRACT

Three flutter suppression control law design techniques are presented. Each uses multiple control surfaces and/or sensors. The first uses linear combinations of several accelerometer signals together with dynamic compensation to synthesize the modal rate of the critical mode for feedback to distributed control surfaces. The second uses traditional tools (pole/zero loci and Nyquist diagrams) to develop a good understanding of the flutter mechanism and produce a controller with minimal complexity and good robustness to plant uncertainty. The third starts with a minimum energy Linear Quadratic Gaussian controller, applies controller order reduction, and then modifies weight and noise covariance matrices to improve multi-variable robustness. The resulting designs were implemented digitally and tested subsonically on the Active Flexible Wing wind-tunnel model. Test results presented here include plant characteristics, maximum attained closed-loop dynamic pressure, and Root Mean Square control surface activity. A key result is that simultaneous symmetric and antisymmetric flutter suppression was achieved by the second control law, with a 24 percent increase in attainable dynamic pressure.

Outline

- Background
- Three Active Controller Designs
  - Modal Rate Feedback
  - Traditional Pole/Zero
  - Modified LQG
- Wind-Tunnel Test Results
- Concluding Remarks

Presented here is an overview of three flutter suppression control law designs. The designs are part of a joint effort by NASA Langley Research Center and Rockwell International Corporation to validate analysis and synthesis methodologies through the development of digital multi-input/multi-output control laws for a sophisticated aeroelastic wind tunnel model.[1,2] The test vehicle used in this effort is the Rockwell Active Flexible Wing wind-tunnel model, modified from its initial configuration through the use of destabilizing wing tip ballasts. The test results refer to testing in the Langley Transonic Dynamics Tunnel conducted in October and November of 1989.

Nature of Wing Flutter

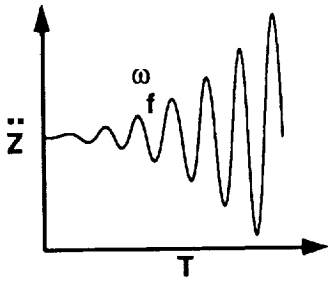

Unstable Time History

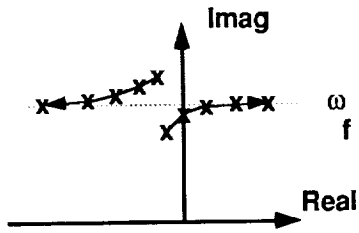

Open-Loop Poles as Function of Dynamic Pressure

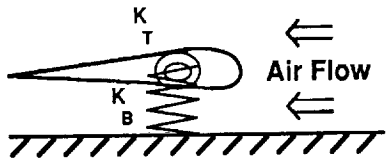

Simple Flutter Model

Wing flutter is a dynamic aeroelastic instability which can be of concern for modern lightweight, flexible, agile fighter aircraft, especially when carrying wing stores. In its classical form, wing flutter is a condition in which bending and torsion vibrations interact with a surrounding air flow in such a way that energy is extracted from the air and drives one of the two modes unstable. The sketch in the upper left depicts an oscillation with a characteristic frequency and divergent growth, as measured by an accelerometer on a wing during flutter. The sketch in the upper right shows that as dynamic pressure increases, characteristic roots of the bending and torsion modes migrate to a common frequency, with one root developing a positive real character indicating exponential growth rather than decay. The schematic of a simple flutter model [3] suggests how an increase in the angle of attack due to the torsion mode would drive the wing tip upward while a decrease in angle of attack due to torsion mode would drive the wing tip downward, in the presence of an air flow, leading to possible instability. The analysis is complicated by the need to model the distribution of mass, inertia, stiffness and damping throughout the wing, as well as quasi-steady and unsteady aerodynamic effects.

ACTIVE FLEXIBLE WING WIND-TUNNEL MODEL

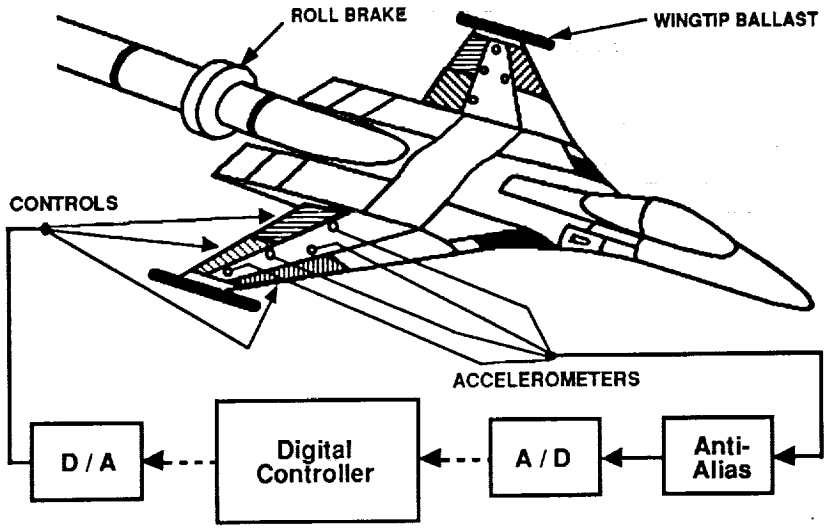

The Active Flexible Wing (AFW) is a full-span, sting-mounted wind-tunnel model with the ability to roll about the sting axis. For the flutter suppression testing in November 1989, the AFW was restricted in roll. The model has a six-degrees-of-freedom force and moment balance on the load path to the sting and has an actuator which can adjust the angle of attack of the model. There are four pairs of control surfaces, as shown in the above figure, with hinge lines near the quarter chord and three-quarter chord locations. The actuators for the control surfaces and for the angle-of-attack adjustment are powered by an onboard hydraulic system. The fuselage of the model is fairly rigid compared with the wings. However, the sting allows some motion up and down and side to side, as well as in torsion.

The three control law designs each used a subset of four pairs of accelerometers and three pairs of control surfaces. Strain gages on the wing are also available but were not used for flutter suppression during the 1989 tests. A digital controller was used to process the signals from the accelerometers to generate commands for the control surface actuators to actively suppress flutter. The accelerometers and actuators are analog devices so that analog-to-digital and digital-to-analog conversions were required.

The original configuration of the AFW was used to study rapid rolling maneuvers for a model with a soft, flexible wing using multiple control surfaces. That configuration did not flutter within the operating range of the Transonic Dynamics Tunnel. Wingtip ballasts were added to the AFW to lower the frequency of the first torsion mode to bring it closer to the frequency of the first bending mode and thereby reduce the dynamic pressure at which flutter occurs to within the range of the wind tunnel.

The tip ballast store, normally coupled in torsion with the wing tip via a hydraulic brake, can be decoupled by releasing the brake and leaving the store restrained in torsion only by a soft spring. Upon brake release the decoupled configuration is flutter free to a much higher dynamic pressure.[4] Thus, the tip ballast store also provides a flutter-stopper capability.

Wind-Tunnel Conditions

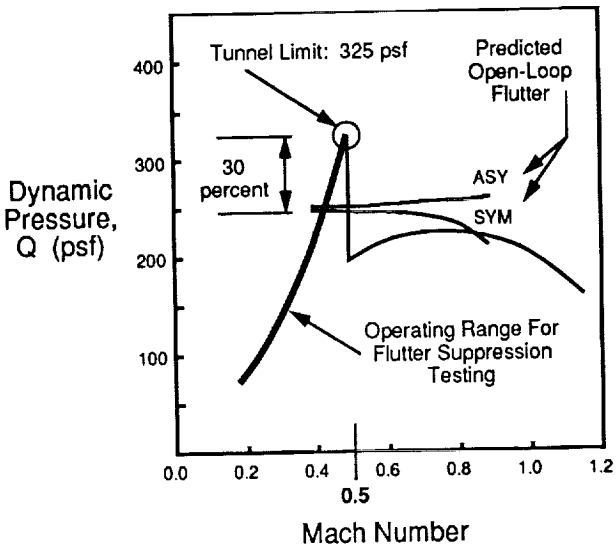

The Transonic Dynamics Tunnel (TDT) is specially configured for testing aeroelastic models.[5] It is a sealed wind tunnel in which Mach number and dynamic pressure can be varied independently by changing motor rpm while simultaneously changing stagnation pressure in the tunnel through the use of pumps. With air as the test medium, as it was for the 1989 test, a maximum dynamic pressure of 325 psf is generated at Mach 0.5 with a stagnation pressure equal to atmospheric pressure. Higher Mach numbers require air to be pumped from the tunnel to reduce the stagnation pressure.

According to analysis prior to the 1989 wind-tunnel entry, when the AFW roll degree of freedom is restrained, the boundaries for symmetric and for antisymmetric flutter occur near the same dynamic pressure, as shown in the above figure. Therefore, a designer must design a control law for each symmetry and plan on having both control laws operate simultaneously.

In order to show the greatest penetration of the AFW flutter boundary within the wind tunnel limits, each control law was designed with the objective of demonstrating closed-loop stability up to the 325 psf condition at Mach 0.5. Although the wind tunnel is capable of changing Mach and dynamic pressure independently, the process of pumping air out of the wind tunnel or bleeding it back in is slower than the process of changing the motor rpm. Also, Mach number effects which are critical in the transonic flight regime are much less significant for Mach numbers at or below 0.5. In the interest of gathering as much data as possible, all flutter suppression control law testing was conducted at a stagnation pressure equal to atmospheric pressure, with Mach number changing as a function of dynamic pressure.

Wind-tunnel turbulence has a direct impact on the expected closed-loop control surface activity for active control flutter suppression, due to control law response to the continual turbulence excitation of the airframe. The magnitude of feedback gains were restricted based upon the control surface rate capability of the AFW and the expected turbulence level in the wind tunnel.

Character of AFW Flutter

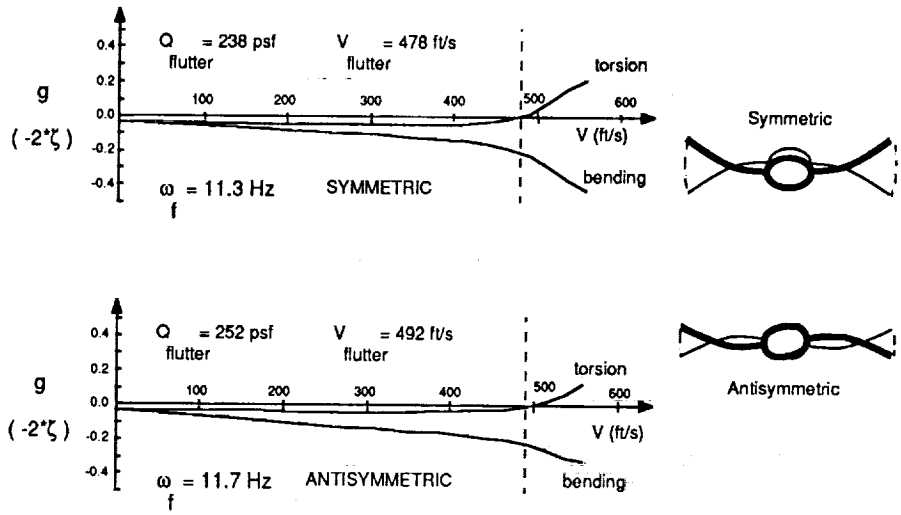

For the AFW, with the roll brake on, the characteristics of the symmetric and the antisymmetric flutter are very similar to each other. This is related to the nearly rigid fuselage and to the mounting conditions. With the roll-brake released (or for a similar vehicle in free flight), the symmetric and antisymmetric flutter would differ significantly from each other. Because of the similarities, a control law designed for one symmetry should require only slight modification in order to be effective for suppression flutter in the opposite symmetry.

The above figure shows a plot of predicted damping as a function of velocity. The damping ratios (ζs) were computed from the eigenvalues of the primary bending and torsion modes for each symmetry, based upon 41st order state-space models for the AFW incorporating 10 second-order structural modes with 1 aerodynamic lag state per mode, 3 third-order actuators, and 1 second-order gust. The plot is shown in a traditional V- g format, where V is velocity and g is the amount of structural hysteresis damping that would be required for neutral stability.[6] The factor of -2 conversion from damping ratio to required hysteresis damping is valid to within 1 percent for the range of values shown here.

Because Mach number effects in the subsonic region were judged to be small, the state space models used to perform the analysis on this page were generated as though a Mach number of 0.5 characterized the air flow regardless of velocity. This approximation is most nearly true as the wind-tunnel operating limit is approached. The symmetric and antisymmetric torsion modes were predicted to go unstable at dynamic pressures of 238 and 252 psf, respectively. The flutter frequency in each case was predicted to be about 11.5 Hz.

At the predicted velocity for onset of symmetric flutter, analysis indicated that the required hysteresis damping increased by 1.7E-3 for an increase in velocity of 1 ft/sec. For the corresponding anti-symmetric case the required hysteresis damping increased by 8.3E-4 for an increase in velocity of 1 ft/sec, indicating the relative predicted onset rates for the two symmetries.

Actuator rate saturation can effectively induce lag and reduce the amplitude of control surface deflections. At the wind-tunnel limit of 325 psf, the open-loop time-to-double for the symmetric flutter mode was predicted to be 1/10 of a second. For this level of instability, actuator rate saturation for even a brief period of time in response to wind-tunnel turbulence could cause unacceptably large growth of the flutter mode. This reinforces the restriction on the magnitude of feedback gains.

Implementation of FSS Control Laws

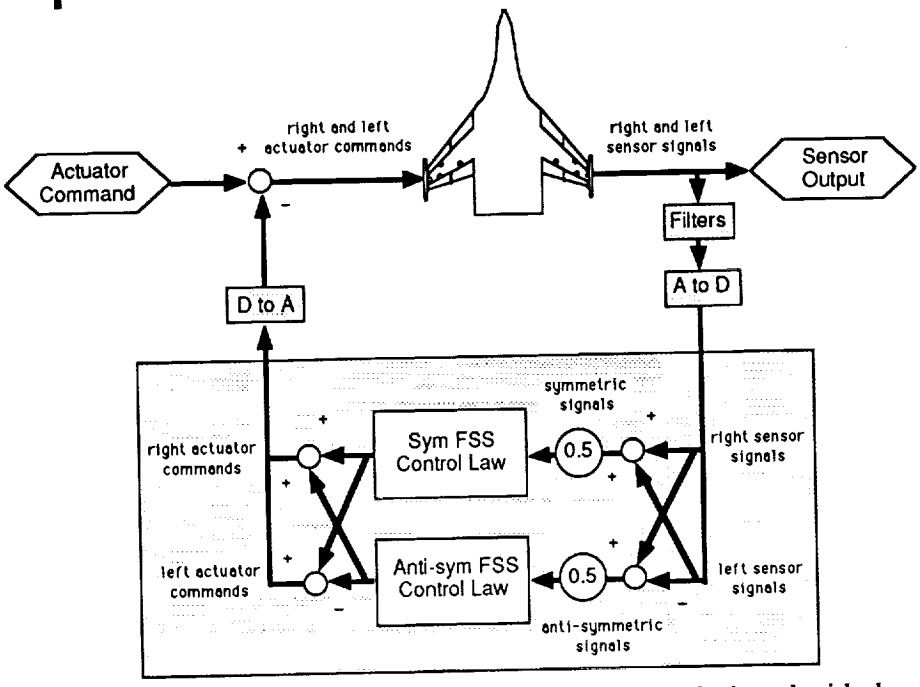

Each of the three Flutter Suppression System (FSS) control laws was designed with the assumption that there was no coupling between symmetric and antisymmetric response for the AFW. The above figure illustrates how the symmetric and antisymmetric forms of the control laws were implemented simultaneously by the digital controller.[7] For each pair of accelerometers, the symmetric signal was determined as the average of the right and left signals and the antisymmetric signal was determined as one half of the difference between right and left signals. Similarly, the right and left control surface commands were determined as the sum and difference of symmetric and antisymmetric commands for each pair of control surfaces.

The digital implementation of the control laws has certain implications for the control law designer. The signal amplitude is quantized in the analog-to-digital and digital-to-analog converters due to finite word length. The sample rate was 200 Hz. An effective 1/2 time step delay on average is introduced by the sampling because after a signal is passed at the beginning of a time step, no additional information is passed until the beginning of the next time step. Computation time required by the digital computer introduces additional delay. The digital-to-analog conversion introduces high frequency transients to the actuators. Finally, an analog anti-aliasing filter is required to attenuate signal strength above 1/2 the sampling rate so that higher frequency harmonic signals are not mistaken for lower frequency signals due to the periodic sampling. A first-order lag at 25 Hz was used for anti-aliasing in preference to a fourth order Butterworth filter at 100 Hz in order to also reduce response to structural modes in the 30 to 40 Hz range.

The trailing edge outboard (TEO) control surfaces tend to be the most effective in controlling flutter, although the actuator hinge moment available for these surfaces is limited compared to the others because of hardware constraints due to the limited space available in the outboard portion of the wing. The leading edge outboard (LEO) surfaces have unfavorable aerodynamic loading which does not tend to restore the surfaces to a neutral position if the actuators become overloaded. The trailing edge inboard (TEI) surfaces have favorable aerodynamic loading, but are not as effective as the TEO surfaces. Each of the wing accelerometer pairs is located near the hinge line of one of the control surface pairs, with the exception of the tip accelerometers (TIP) which are located approximately mid-chord near the wing tip. The tip accelerometers tend to respond most strongly to the flutter mode, while at the same time being relatively insensitive to the higher frequency modes when compared with the inboard accelerometers.

Flutter Suppression System . . .

Design Objective

- Increase in Flutter Q: 30 percent

Design Requirements

- Gain Margin: +/- 6 dB
- Phase Margin: +/- 30°
- $\dot{\delta}$ RMS: < 75°/sec (= 1/3 of max)
- δ RMS: < 1.0° (= 75°/sec at 11.5 Hz)

The design objective for all three flutter suppression control laws was to demonstrate closed-loop stability up to the wind tunnel limit of 325 psf dynamic pressure. This would constitute a 30 percent increase in the flutter dynamic pressure relative to the lowest predicted open-loop flutter boundary in the subsonic region. Because of the similarity between the symmetric and antisymmetric flutter, the control law designs in the following sections are presented as though only one symmetry were involved.

For those control laws which could be represented by single-input/single-output (SISO) gain and phase margins, a predicted gain margin of +/- 6 decibels and a predicted phase margin of +/- 30° was to be maintained throughout the test envelope, according to pretest analysis. The control law which required multi-input/multi-output (MIMO) analysis was judged by potentially conservative multi-variable margins and the stated requirements were slightly relaxed for that case.

The trailing edge outboard control surfaces were predicted to have a peak no-load rate capability of 225°/sec. It is desired that no rate saturation occur. If one accepts no rate saturation for a 3 standard deviation turbulence intensity as adequate for assuring no rate saturation,[8] this constrains the Root Mean Square (RMS) rate for a 1 standard deviation turbulence intensity to be less than 75°/sec. At a predicted flutter frequency of about 11.5 Hz, this translates to a maximum RMS control deflection of 1.0°.

A fifth requirement for evaluating candidate control laws prior to the wind tunnel entry was to be able to demonstrate closed-loop stability throughout the test envelope using a batch simulation. The simulation replicated quantization effects due to finite word length in the signal converters and imposed rate and displacement limits on the control surface actuators. The simulation also allowed both symmetries to be run simultaneously in the presence of simulated turbulence excitation with a separate dynamic actuator model for each of the control surfaces. The actuator models were based upon measured actuator frequency response data. Variations in the actuators introduce a possible source of nonsymmetry or coupling between the symmetric and the antisymmetric cases for the closed-loop system. While this nonsymmetry was generally neglected during design, these effects were addressed during control law evaluation by means of the simulation.

Modal Rate Feedback

Adams/Christhilf

- Design Philosophy:
  - Synthesized flutter mode rate
  - Fixed controller dynamics
  - Optimized sensor & control coefficients

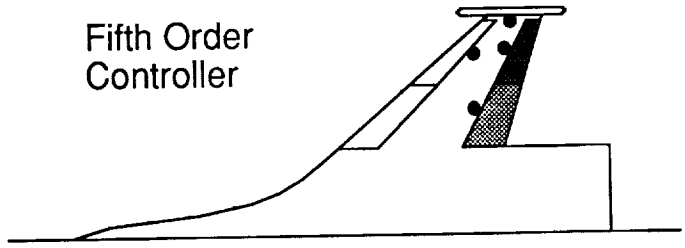

The control law designed and tested by Adams and Christhilf can be described as using modal rate feedback. The design philosophy for the Modal Rate Feedback control law is to use linear combinations of multiple accelerometer signals together with dynamic compensation to synthesize the flutter mode rate for feedback to multiple control surfaces.[9] Multiple sensors are used to identify the activity of the flutter mode not only by frequency, but also by the geometry of its characteristic mode shape. Multiple control surfaces are used in an effort to control the flutter mode exclusively. The coefficients used for the accelerometer pairs, the control surface pairs, and the overall system gain are generated using an optimization procedure. The four pairs of sensors used were the TIP, TEO, LEO, and TEI and the two pairs of control surfaces used were the TEO and TEI, as shown in the above figure.

The controller dynamics were set by the control law designer. Two first-order lags with break frequencies lower than the frequency of the flutter mode were used to act as stable integrators in order to transform modal acceleration into modal rate and position. A first-order "washout" filter with a zero at the origin and a pole at a frequency below the flutter frequency was used to reduce response to steady state bias errors. Finally, a second-order notch filter was used to adjust the phasing of the control action at the flutter frequency and to reduce the response to a nonflutter mode. (The notch for the symmetric case was for a 5.7 Hz sting mode and the notch for the antisymmetric case was for an 18.3 Hz structural mode.)

The method for generating the comparison between predicted and desired response for use in the optimization required individual frequency responses for each accelerometer pair due to excitation by each actuator pair. These can be obtained either through pretest modeling or through experiment.[10] Experimentally derived frequency responses were in fact used during the 1989 wind-tunnel entry to improve the control law.

Flow Chart

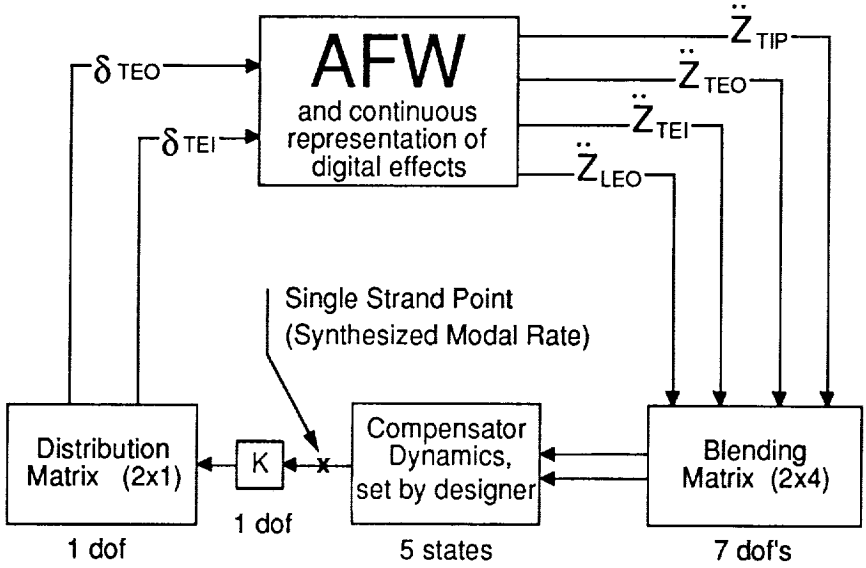

The signals designated in the above figure as δs and $\ddot{z}$'s represent commanded control surface deflections and measured local accelerations for a given symmetry. The frequency response for each acceleration signal due to each control surface command (symmetric or antisymmetric) for continuous models of the AFW at several dynamic pressures were precomputed for the frequency range from 2 to 64 Hz and were retained for further analysis. For the purpose of control law design, frequency responses representing the effects of the time delays and of a candidate set of analog filters and compensator dynamics were also computed and combined with the frequency responses that represented the AFW.

The coefficients of the blending and distribution matrices were used to generate linear combinations of the frequency responses. The blending matrix was actually used to form two dynamically distinct linear combinations. The difference between these two is that one was formed as a linear combination of frequency responses that contained the effect of only one integrator, and the other was formed as a linear combination of frequency responses that contained the effect of two integrators. When implemented in the wind-tunnel test, the discrete state-space equation used to specify the compensator dynamics was set up in such a way that one of the two inputs to the compensator bypassed the second integrator, with the output of the compensator being the sum of the two signals.

The purpose of the blending matrix was to take four local acceleration signals and synthesize two signals, each roughly corresponding to the acceleration of the flutter mode. The purpose of the distribution matrix was to take a single command signal, intended to control the flutter mode, and distribute that command to multiple control surfaces. Isolation of the flutter mode was determined in part by the analog filtering and compensator dynamics, and in part by the extent to which the blending and distributing rejected feedback interaction with other modes.

Although there are 8 and 2 coefficients in the blending and distribution matrices, the magnitude of the largest coefficient of each matrix was factored into a system gain, so that the normalized blending and distribution matrices had 7 and 1 degrees of freedom, respectively, which together with the system gain constituted the 9 degrees of freedom in the formulation of an objective function for an optimization procedure. The output from the dynamic compensator is a single strand point for the feedback path, and the optimizer was used to drive the composite frequency response at that point to match a simple, desired frequency response. The frequency responses representing the compensator dynamics were computed prior to the optimization and the parameters of the compensator dynamics were not optimized.

Optimization Strategy

Antisymmetric, Q = 325 psf

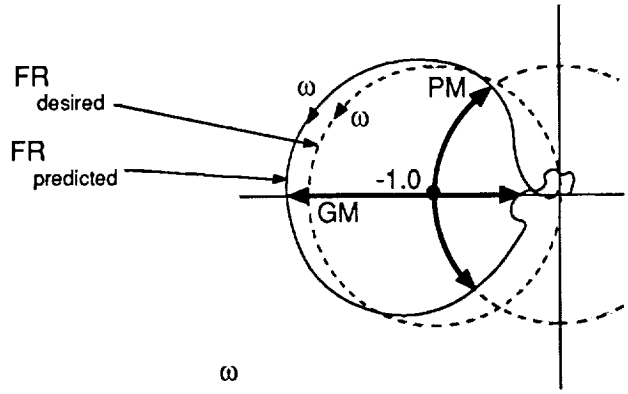

$$\text{Cost Function} = \sum_{\omega=\omega_{min}}^{\omega_{max}} \left(W_{\omega} * \left(FR_{predicted} - FR_{desired} \right)_{\omega}^{2} \right)$$

The above figure shows a Nyquist plot, or a polar plot of the open-loop frequency response, for the sensor output due to commanded control deflections as defined at the single-strand point. The frequencies used in the AFW analysis span from 2 to 64 Hz. A full Nyquist plot would span frequencies from minus infinity to plus infinity, but the portion of the plot for negative frequencies is symmetric about the real axis to the portion of the plot for positive frequencies so that the information is redundant. The Nyquist stability criterion requires that for each unstable pole of the open-loop system, the Nyquist plot must form one counterclockwise encirclement of the -1 point in order for the closed-loop system to be stable. For oscillatory instabilities, the unstable poles occur in complex conjugate pairs, requiring two encirclements per pair. However, one of the encirclements would occur for the frequency range from minus infinity to zero, which is not shown.

In the case of actively stabilized flutter, the encirclements will occur in the vicinity of the flutter frequency. Gain and phase margins can be read directly from a Nyquist plot as the amount of shift which can be tolerated while still encircling the -1 point. Excess lag at the flutter frequency will shift the positive frequency plot clockwise (and the negative frequency plot counterclockwise) until closed-loop instability is encountered at a frequency slightly above the flutter frequency. Similarly, excess lead results in closed-loop instability at a frequency slightly below the flutter frequency.

The response of modes other than the flutter mode will be evident as additional "lobes" on the Nyquist plot. To the extent that the sensor and control surface blending can isolate the flutter mode, these extra lobes will be small. If these lobes are not small, they can result in clockwise encirclements of the -1 point, indicating that a previously stable mode has gone unstable at a frequency other than the flutter frequency.

The desired frequency response is the response that would result from using rate feedback to stabilize an unstable sinusoidal oscillator. The cost function for the optimization is the sum of the squares of the difference between the predicted and the desired response, weighted with frequency. The weights were chosen to emphasize the flutter frequency. Since the frequency response is complex, the "squaring" is done using complex conjugates, resulting in a real number for the value of the cost function. A Davidon-Fletcher-Powell optimization routine[11] was used to find the system gain and blending and distribution matrix coefficients for which the cost function was minimized at a particular dynamic pressure. Each resulting design was evaluated at other dynamic pressures to see that predicted performance was satisfactory throughout the wind-tunnel test envelope.

Control Surface Rates

Closed-Loop, Symmetric, Q = 300 psf

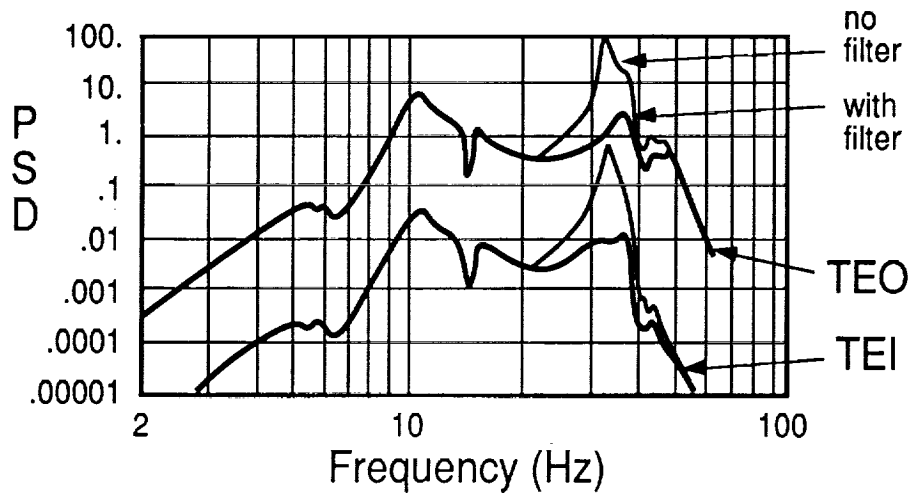

RMS Rates (°/sec) ⟹

	No Filter	With Filter
TEO	138	52
TEI	11	4

To model turbulence, a Dryden gust spectrum was used which has a nonzero value at zero frequency, rises 12 percent to a peak at a frequency of 10 Hz, and decreases monotonically to zero at higher frequencies. An overall RMS turbulence intensity of 1 ft/sec was judged to be a reasonable estimate of the turbulence in the wind tunnel, and this was apportioned as 85 percent symmetric and 15 percent antisymmetric. This gust spectrum was applied to assumed symmetric and antisymmetric gust mode shapes in order to model the effect of the turbulence on the wind-tunnel model.

The above figure shows a power spectral density (PSD) plot for closed-loop rates for the TEO and TEI control surfaces due to the modeled turbulence at a dynamic pressure above the open-loop flutter point. (This is shown as a representative example and does not depict the PSD for the control law actually tested.) The control surface RMS rates in °/sec can be calculated as the square roots of the areas under the curves when plotted on linear scales.

If the symmetric and the antisymmetric responses to turbulence were completely uncorrelated, the total control surface activity would be the square root of the sum of the squares of the symmetric and antisymmetric control surface activity. For design purposes the components were assumed to be constructively correlated so that straight addition was used to estimate the total activity. The figure shows response predicted for 1 ft/sec symmetric turbulence, which would be scaled 85 percent before combining with the antisymmetric turbulence response. The design limit for total control surface activity was chosen to be 75 °/sec, consistent with predicted actuator rate limits.

The figure shows a local peak in the control surface activity at a frequency of about 11.5 Hz. This represents the activity required to suppress the unstable flutter mode as it is excited by turbulence. The figure also shows significant control surface activity in the frequency range from 25 to 40 Hz which results from nonproductive response to excitation of higher frequency structural modes. In order to reduce control surface activity, an analog band-reject filter was used. This filter consists of three fairly broad second-order notches with center frequencies at 32, 40, and 49 Hz. The band-reject filter was used instead of a low-pass filter in order to keep the resulting lag at the flutter frequency to a minimum, while still achieving the desired attenuation. The lag at 11.5 Hz due to the filter is about 28°.

Predicted Performance
Modal Rate Feedback

		At 300 psf		Control Activity (percent of max allowed RMS)	
	Max Q	+/- GM	+/- PM	TEO	TEI
SYM	>325	9 dB	34 °	67 percent	25 percent
ASY	>325	12 dB	49 °		

The above figure shows predicted performance for the modal rate feedback controller resulting from linear analysis and substantially confirmed by nonlinear batch simulation. "Max Q" refers to the maximum dynamic pressure, measured in psf, for which the closed-loop system was predicted to be stable for both linear analysis and simulation. Gain margins and phase margins are shown at a dynamic pressure of 300 psf, which was chosen as a common evaluation point for the three control laws tested. Margins were predicted by linear analysis to meet the stated requirements throughout the wind-tunnel test envelope. Gain margins were verified in simulation at selected dynamic pressures by varying symmetric and antisymmetric system gains individually until simulation time histories showed divergence. The gain margins obtained from simulation were comparable to those obtained through linear analysis. Phase margins were not verified through simulation.

The percentage of maximum allowed control surface activity is relative to the designated maximum RMS control surface rate of 75 °/sec. The predicted RMS control surface rate was determined by using the batch simulation with simultaneous symmetric and antisymmetric turbulence excitation. The simulation indicated that the specified control surface rate limit was not exceeded for either pair of control surfaces. It also shows significant activity on the TEO and TEI surfaces, although the TEO surfaces dominate.

Traditional Pole/Zero Design

Srinathkumar/Waszak

- Design Philosophy:
  - Simplify problem
  - Develop understanding
  - Design controller as simple as possible

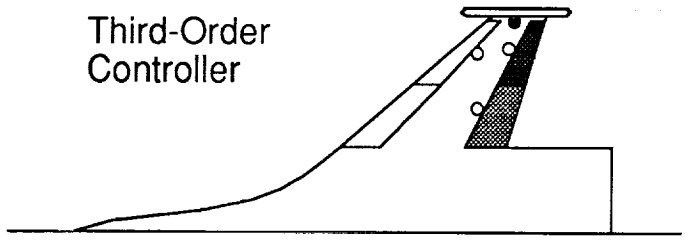

The control law designed and tested by Srinathkumar and Waszak is generated using traditional complex plane mappings of poles and zeros. A driving philosophy behind this design effort is to avoid getting lost in complexities which are of secondary importance with respect to the flutter control problem and to reduce the problem to its bare essentials. One step toward accomplishing this is to concentrate primarily on the two structural modes that participate directly in the flutter and on the SISO zeros in the same frequency range which result from the choice of a particular sensor pair and control surface pair. Sting modes and their associated zeros are ignored, as are higher frequency modes. This is possible due to fortuitous effective pole/zero cancellations associated with chosen control surfaces and sensors, and also due to frequency separation between the flutter dynamics and higher order modes.

Selection of sensors and control surfaces was a necessary first step in the controller design. The accelerometer pair at the TIP location was chosen because it is the pair most responsive to the flutter and also least responsive to higher frequency modes. The TEO control surface pair was chosen as being the most effective in controlling flutter without the danger of going "hard over" if the actuator hinge moment capability is exceeded. The TEI control surface pair was added later to reduce the TEO control surface activity. The commands sent to the TEO and TEI surfaces were dynamically equivalent in that they differed only by a constant gain factor so that SISO design and analysis techniques could still be used.

Straight feedback with no dynamic compensation was investigated first to see whether this would be sufficient to stabilize the system, and if not, what problems would be encountered when attempting to employ a simple solution. Consideration of the high gain required and the desire to ensure a favorable root locus path led to the use of a second-order "dipole" filter to be described later in this section. A final consideration was that the response of the system to steady state bias errors must be acceptably small, leading to the addition of a first-order washout filter and bringing the controller order up to three.

Critical Zero

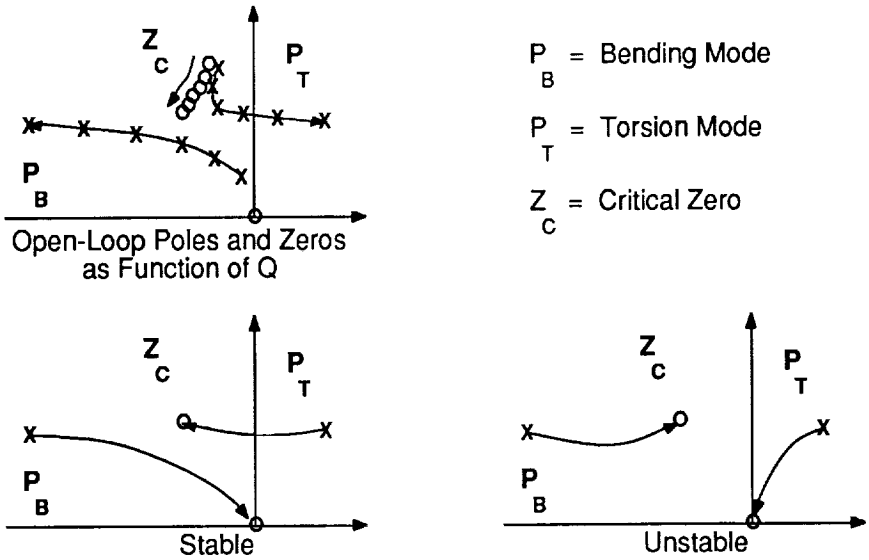

For the sketches of poles and zeros presented above for this design, the horizontal axis is greatly exaggerated relative to the vertical axis in order to show more detail. All poles and zeros not associated with the compensator should be considered to lie near the imaginary axis. The sketch in the upper left shows a locus of poles and zeros as a function of dynamic pressure. The poles represent the bending and torsion modes for the AFW with no active compensation, and the zeros arise from a particular choice of sensors and actuators. The pair of zeros at the origin results from the fact that accelerometers were used for feedback. It was found that for the TEO control surface and the TIP sensor, there is a critical zero which is closely associated with the torsion mode. Note that as dynamic pressure increases the critical zero and the pole associated with the torsion mode tend to stay near each other until just below the flutter dynamic pressure at which point the pole breaks away to the right, crossing into the right half of the complex plane and indicating instability.

The use of simple feedback will drive the closed-loop roots from the open-loop poles to the transfer function zeros, as a function of feedback gain. However, given uncertainties in the model of the plant it is not always clear what path the roots will take.[12] For the lower two figures, the one on the left shows how the system might be stabilized by simple feedback whereas the one on the right shows a case where there is no value of gain for which the closed-loop system will be stable.

Even when the desired path is followed, the location of the isolated critical zero near the imaginary axis indicates that a high gain would be required to drive the unstable root close enough to the zero to stabilize the system with sufficient damping. One difficulty associated with high-gain controllers is that the control surface rates required to control the flutter while subject to continual turbulence excitation would be large and threaten to saturate the capability of the actuators, causing loss of control of the flutter. Another difficulty associated with high-gain controllers is that higher frequency modes or actuator roots can be driven unstable.[13]

Dipole Filter

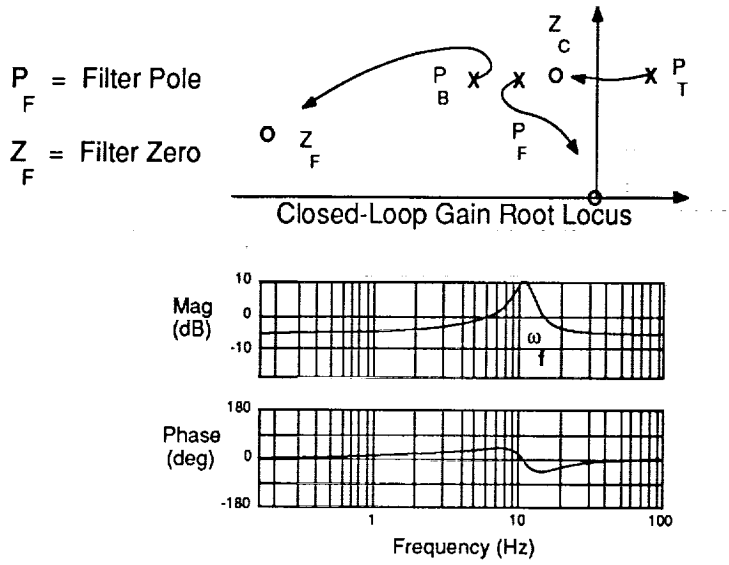

Dipole Filter Dynamics

In order to reduce the feedback gain required for stabilization due to the location of the critical zero near the imaginary axis, dynamic filtering is required. The intent for this control law is to "soften" the effect of the critical zero by placing a filter pole near the critical zero and placing a filter zero further to the left. The result is similar to an inverted notch and will be referred to as a dipole filter.

The location of the critical zero changes as a function of dynamic pressure, whereas the location of the open-loop filter pole is independent of dynamic pressure unless scheduling of dynamic parameters is used. Also, the locations of system zeros are difficult to predict analytically and can be difficult to measure experimentally. In the interest of avoiding scheduling and due to the uncertainty about the exact location of the critical zero, the filter pole is placed somewhat to the left of the predicted critical zero, with a damping ratio of about 10 percent. Using frequency domain Nyquist criteria for stability margin analysis, a 50 percent damping ratio at a natural frequency 20 percent higher than that for the compensator pole can be shown to be a good choice for the compensator zero location.

The lower portion of the figure shows magnitude and phase plots of the frequency response of the dipole filter by itself. It can be seen that the dipole filter amplifies the control surface activity in the frequency range predicted for flutter, which in this case is about 11.5 Hz. Because the control surface activity is concentrated at this frequency, the controller makes efficient use of the available control power and is fairly insensitive to modeling errors outside the frequency range of interest.

Note that although pole/zero cancellation is generally thought to be sensitive to having accurate knowledge of the plant, the dipole filter was evaluated using variations in the model of the AFW and it was judged to be tolerant to changes in the frequency of the flutter mode. This is due in part to the "robust" placement of the filter pole with respect to the critical zero, with the result that the stabilizing character of the root locus did not change despite the frequency shifts.

Predicted Performance
Traditional Pole/Zero Design

		At 300 psf		Control Activity (percent of max allowed RMS)	
	Max Q	+/- GM	+/- PM	TEO	TEI
SYM	>350	7 dB	33°	73 percent	3 percent
ASY	>350	7 dB	38°		

As with the previous control law, the traditional pole/zero design was predicted through analysis and simulation to provide closed-loop stability up to the limit of the operating range of the wind tunnel. The gain and phase margins at the common evaluation point compare favorably with the requirements, and the required margins were predicted through linear analysis to be maintained throughout the test envelope. Positive and negative gain margins were verified through simulation. Phase margins were more difficult to determine from simulation, and only tolerance to phase lag was estimated. This was done by reducing the break frequency on a simulated 100 Hz fourth-order Butterworth anti-aliasing filter until simulation time histories showed oscillatory divergence, and determining the resulting lag at the predicted flutter frequency. The 100 Hz fourth-order Butterworth filter was used instead of the first-order 25 Hz anti-aliasing filter for this analysis.

The rate limit constraints of the actuators were not violated. It can be seen from the percent of maximum allowed control surface activity as shown in the above figure that although the TEO and TEI surfaces were both used, clearly the dominant activity is on the TEO surfaces.

In order to test the robustness of this control law design to parametric uncertainties, the control law was analyzed for closed-loop stability for a variety of wind-tunnel conditions which were not part of the planned wind-tunnel test envelope. Specifically, an early version of the control law was designed for a Mach number of 0.9 in Freon and was evaluated at a Mach number of 0.8 in Freon, and 0.5 in air. This early control law was designed to suppress symmetric flutter, but was used with only minor modifications to evaluate its effectiveness for suppression of antisymmetric flutter for each of the listed wind-tunnel conditions. In each case the closed-loop system was predicted stable up to at least 325 psf.

Modified LQG

Mukhopadhyay

- Design Philosophy:
  - Start with optimal minimum energy design
  - Simplify controller
  - Improve MIMO robustness

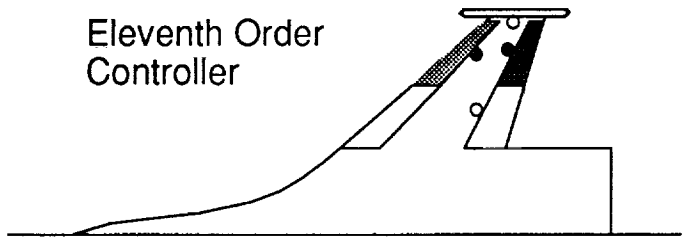

The control law designed and tested by Mukhopadhyay is designed using a modified Linear Quadratic Regulator procedure with a state estimation for output feedback. The philosophy behind this control law design is to exploit MIMO degrees-of-freedom through a systematic procedure which allows the designer to perform trade-offs between desired closed-loop performance and considerations of control surface activity.[14] This method is truly multi-input/multi-output and requires the use of singular values for stability margin analysis rather than SISO gain and phase margins. The inputs to the procedure were modified by the designer to improve the robustness to uncertainty in the modeling of the plant. These modifications were based upon singular values or on equivalent MIMO measures of gain and phase margins which can be derived from singular values.[15]

The Linear-Quadratic-Gaussian (LQG) method used here results in a controller with a large number of states so that controller order reduction is required for implementation. After order reduction the Modified LQG design had 11 states per symmetry. The trailing-edge-outboard and leading-edge-outboard control surfaces were used, as well as their co-located accelerometers.

Design Steps

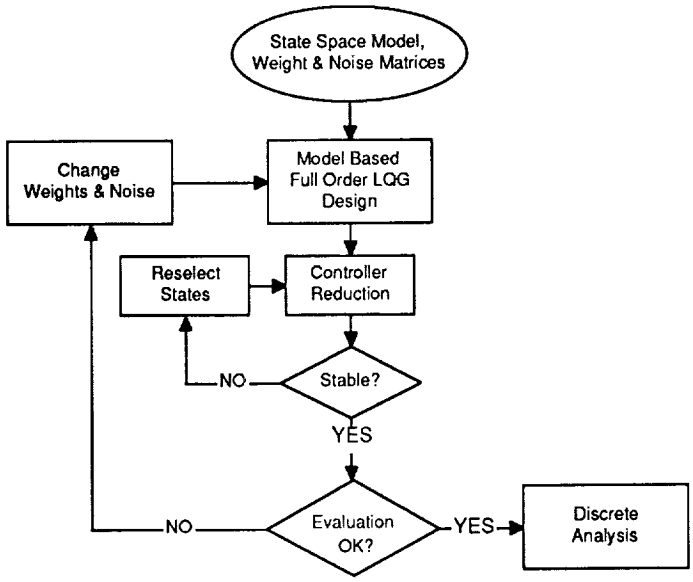

The LQG procedure uses a plant state-space model and weight and noise covariance matrices to generate a model-based, full-order compensator. For a design point at a wind-tunnel condition for which the open-loop plant is unstable, a full-state-feedback optimal regulator was designed with a zero weighting matrix for the states and an identity weighting matrix for the controls. This regulator has the property that for the closed-loop system the unstable characteristic roots are reflected into the left half plane while all other roots remain unchanged, and represents the minimum control energy solution for stabilizing the plant.[16] A model-based minimum variance state estimator was also designed with 0.000001 radian plant input noise, 1/12 foot-per-second gust input noise and 0.32 ft/sec^2 (0.01 g) measurement noise.

The full-state-feedback regulator was combined with the state estimator to generate a full-order compensator which uses only sensor feedback with no direct knowledge of the states of the plant. Based on nonminimum phase transmission zeros contained in the state-space model and many poorly controllable and observable states for the control surfaces and sensors used, the noise intensities were chosen after a few trials so as to produce a low-gain LQG control law which stabilized the plant and itself had stable characteristic roots.

The next step was to reduce the order of the control law. The full-order LQG control law was reduced through a process of balanced realization and modal truncation, based in part upon evaluation of modal residues.[17] Although a lower-order stabilizing control law could be found, a tenth-order control law was chosen since its performance was close to the performance of the full-order LQG control law. An 11th state was added as part of a washout filter used to attenuate the response to bias errors.

When a stable reduced-order control law was found, the full-order and the reduced-order control laws were analyzed and the singular values, frequency responses, and RMS control surface activity were compared. Based upon this overall evaluation, modifications were made to the LQG weight and noise covariance matrices to improve robustness to modeling errors and to meet constraints. The final step was to discretize the continuous control law at a sample rate of 200 samples per second using Tustin transformations and perform further analysis.

Poles as Function of Q
Symmetric

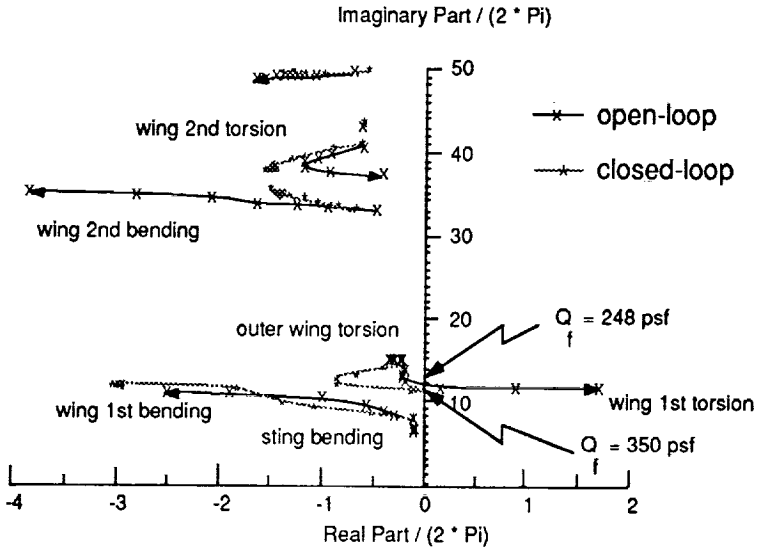

The above figure shows the plant open-loop poles and fixed-gain, closed-loop roots as functions of dynamic pressure. To simplify the figure, compensator poles and roots are not shown. Although the open-loop compensator poles do not change as a function of dynamic pressure, the compensator roots interact with the roots of the plant in the presence of feedback and therefore change with dynamic pressure. However, for this design the compensator poles are stable open-loop and the compensator roots are stable closed-loop for the dynamic pressure range shown.

Typically the poles for the full-order compensator will be located in the same frequency ranges as the poles for the open-loop plant. During compensator order reduction, compensator poles above about 25 Hz were removed since they tended to have little effect on the control of flutter at 11.5 Hz. However, it was found through singular value analysis that the stability margins in the frequency range around 32 Hz needed improvement. Since the open-loop plant poles in this region are stable, an analog notch filter with a center frequency of 32 Hz was used to prevent the compensator from driving the modes in this region unstable.

The solid lines indicate the paths of the open-loop poles and the shaded lines indicate the paths of the closed-loop roots. The crossing point where the 11.5 Hz flutter mode goes unstable is identified in the figure as 248 psf for the design model of the symmetric plant with no compensation and 350 psf for the symmetric plant with compensation.

Predicted Performance
Modified LQG

		At 300 psf *		Control Activity (percent of max allowed RMS)	
	Max Q	+/- GM	+/- PM	TEO	LEO
SYM	350	3 dB	18°	62 percent	26 percent
ASY	325	4 dB	20°		

* Equivalent multi-variable margins for simultaneous changes on all channels

The Modified LQG control law was predicted through analysis and simulation to provide closed-loop stability up to the limit of the operating range of the wind tunnel. The gain and phase margins shown here represent guaranteed minimum margins for simultaneous variations on multiple channels. These margins can be conservative if they represent an unlikely combination of variations. The margins shown here do not meet the requirements for SISO gain and phase margins. However, because of their potential conservative nature, these margins were judged to be sufficient for testing the control law.

The closed-loop RMS control surface rates in the presence of random gust excitation are within the specified limits. The percent of maximum allowed control surface activity for each pair of surfaces indicates that both the TEO and LEO control surface pairs are used to a significant extent, with the TEO surfaces being the dominant surfaces.

Measured vs Predicted Behavior

Symmetric, Q = 175, Open-Loop, Plant Only

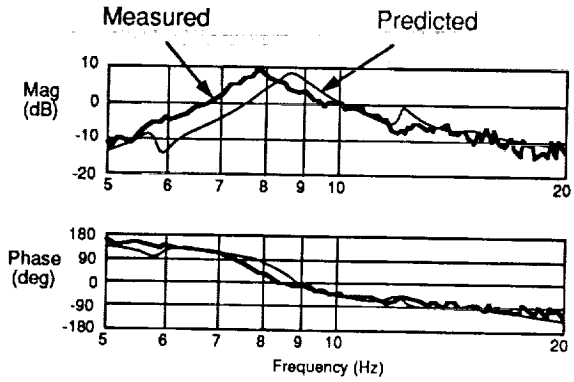

	Q f (psf)	ω f (Hz)
Measured	220	9
Predicted	248	11

Frequency Response for $\ddot{z}_{TIP}$ due to δ_{TEO}

One thing found during the wind-tunnel test was that the wind-tunnel model did not behave quite as predicted. One difference which became evident early in the testing was that the frequencies at which dominant frequency response peaks occurred were somewhat lower than predicted. For a dynamic pressure of 175 psf, the above figure shows a frequency shift of about 1 Hz for the bending mode for the symmetric case. Prior to the wind-tunnel test, the analytical model had been adjusted so that the frequencies at zero dynamic pressure matched the frequencies measured during a ground vibration test (GVT). The differences between predicted and measured frequencies must, therefore, be related to aerodynamic effects.

The dynamic pressure for zero damping of the flutter mode was also found to be lower than predicted by about 30 psf or 13 percent. Large open-loop structural response was encountered in the wind tunnel at a dynamic pressure of about 220 psf and has been judged to be primarily antisymmetric. Analysis indicated that symmetric flutter would occur first at about 248 psf, with antisymmetric flutter occurring at about 252 psf.

Since none of the control laws were scheduled with dynamic pressure, it is more significant to compare the difference between measured and predicted flutter frequencies at corresponding flutter dynamic pressures than it is to compare the difference between measured and predicted frequencies at a given dynamic pressure. This means that the relevant frequency shift for the control law designers was about 2 Hz, as shown in the chart.

The phase characteristics of the response shown in the figure indicate a frequency shift consistent with the frequency shift for the peak magnitude. In fact, a Nyquist plot for the measured and predicted open-loop responses shown here would be almost identical because the phase angle for the peak response is nearly the same for the two and the frequency shift would not be apparent. However, if a control law has dynamics in the flutter frequency range, the shifted plant dynamics can interact with the controller dynamics to introduce potentially large phase shifts. Therefore a control law designer should be aware of the effects of changes in frequency for critical modes, and not rely strictly on phase margins.

Maximum Q Obtained

Closed-Loop Testing

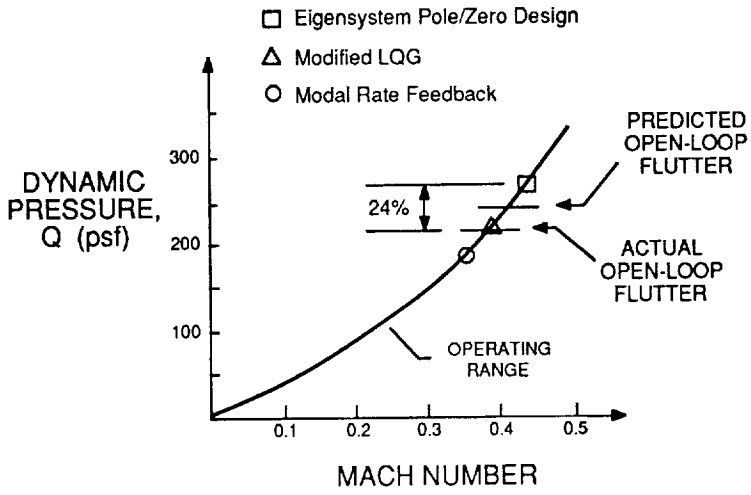

The above figure shows the highest closed-loop stable dynamic pressure achieved by each control law. Notice that the open-loop plant goes unstable at a dynamic pressure lower than expected, at about 220 psf rather than 248 psf.

The Traditional Pole/Zero design demonstrated closed-loop stability up to a dynamic pressure of about 272 psf. This represents an increase of about 24 percent relative to the observed open-loop flutter boundary. The controller stabilized the model at the 272 psf condition for several minutes while time histories for loads and for commanded control deflections due to tunnel turbulence were being recorded for RMS analysis. The wind-tunnel safety system was activated automatically after the model responded to a burst of turbulence and the structural loads exceeded preset limits. Since the control law was able to limit the amplitude of the flutter mode for lower turbulence levels, it is quite possible that increasing the feedback gain would keep the structural loads due to turbulence within the prescribed limits, at least in the flutter frequency range.

The Modified LQG controller did not significantly change the observed flutter dynamic pressure relative to the open-loop case. The closed-loop control surface activity due to turbulence for this controller was lower than anticipated, suggesting that a higher gain solution might achieve flutter suppression with an acceptable increase in control surface activity.

The Modal Rate Feedback caused a large structural response at a dynamic pressure below the open-loop flutter boundary. At the start of the flutter suppression testing for this control law, experimentally derived open-loop controller performance evaluation (CPE) at 125 psf and 175 psf indicated that closing the loop would drive the system unstable. The primary cause for this was undue sensitivity to frequency shifts of the critical structural modes due to the design of the controller dynamics. However, since the method is able to use experimentally derived frequency responses as inputs to the optimization, the frequencies of the controller dynamics were shifted to match the observed shift and the blending and distribution matrices were reoptimized using data collected at 125 and 175 psf. Subsequent open-loop CPE and closed-loop testing with the redesigned controller showed that the system performed as expected at 125 and 175 psf. The large response occurred at 185 psf at a frequency of about 7 Hz. The cause for the large response has not been determined, but it may have been related to differences between the left and right actuators for the TEI control surfaces.

RMS Control Rates

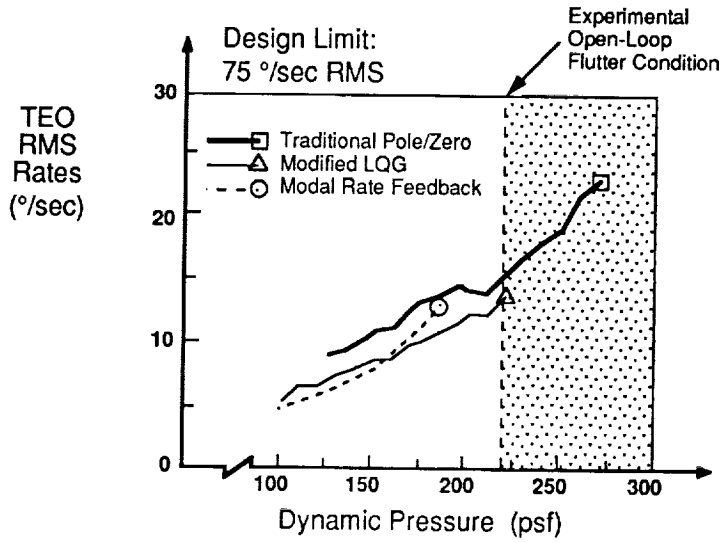

The above figure depicts closed-loop control surface RMS rates as functions of dynamic pressure. The RMS rates were synthesized from commanded deflections since rates were not commanded directly. The three curves represent the measured response for the three control laws during testing. Since the TEO control surfaces were dominant for each control law, rates are shown for the TEO surfaces. If there was a difference between the RMS value for the left surface and the RMS value for the right surface, the maximum of the two is shown.

Note that all three control laws command about the same level of control surface activity for the dynamic pressures tested. This reflects the fact that all three were designed with the same turbulence model and the same design limits. Note also that none of the control laws had difficulty staying within the design limit of 75°/sec RMS. In fact, the peak measured rate is only about 1/3 of the limit for the Traditional Pole/Zero design at 272 psf. This suggests that the turbulence levels used for design should be reduced prior to the next wind tunnel entry to allow more use of the available control power.

Concluding Remarks

- Three FSS control laws designed and tested
- Analysis predicted that all three would meet objective
- Wind-tunnel model behaved differently than expected
- One FSS control law demonstrated flutter suppression to 24 percent above open-loop flutter dynamic pressure

Three flutter suppression control laws were designed for the Rockwell Active Flexible Wing. The control laws were implemented digitally and tested subsonically in the Transonic Dynamics Tunnel at NASA Langley Research Center. All three control laws were predicted to meet the objective of significantly raising the flutter onset dynamic pressure, while maintaining stability margins and not violating control surface rate and displacement limits. Wind-tunnel testing generally confirmed the analytical predictions for the open-loop character of the AFW, although differences were observed. Of the control laws tested, only one was sufficiently robust to the observed differences to raise the flutter dynamic pressure. The Traditional Pole/Zero Design was able to demonstrate simultaneous symmetric and antisymmetric flutter suppression for several minutes at a dynamic pressure 24 percent above the observed open-loop flutter boundary, in the presence of turbulence.

The 1989 wind-tunnel test has provided data for assessing the fidelity of the analytical models of the AFW and for evaluating the robustness of the control laws to "real world" implementation considerations. Data is available for upgrading the mathematical models of the AFW for possible distribution to other control law designers. Further, the AFW project team has had an opportunity to work together in a multidisciplinary effort involving aeroelastic modeling and simulation, control law design and analysis, digital controller implementation, and near-real-time controller performance evaluation.

References

1 Noll, T., Perry, B. III, et al.: "Aeroservoelastic Wind-Tunnel Investigations Using the Active Flexible Wing Model - Status and Recent Accomplishments," NASA TM-89-101570, April 1989.

2 Perry, B. III, Mukhopadhyay, V., et al.: "Design, Implementation, Simulation, and Testing of Digital Flutter Suppression Systems for the Active Flexible Wing Wind-Tunnel Model," ICAS Paper No. 90-1.3.2, September 1990.

3 Horikawa, H. and Dowell, E. H.: "An Elementary Explanation of the Flutter Mechanism with Active Feedback Controls," Journal of Aircraft, Vol. 16, April 1979, pp. 225-232, AIAA 79-4049.

4 Reed, W. H. III, Cazier, F. W. Jr., and Foughner, J. T. Jr.: "Passive Control of Wing/Store Flutter," NASA TM-81865, December 1980.

5 Staff, NASA LaRC: "The Langley Transonic Dynamics Tunnel," Langley Working Paper, September 1969.

6 Garrick, I. E. and Reed, W. H. III: "Historical Development of Aircraft Flutter," Journal of Aircraft, Vol. 18, November 1981, pp. 897-912, AIAA 81-0491R.

7 Hoadley, S. T., Buttrill, C. S., McGraw, S. M., and Houck, J. A.: "Development, Simulation Validation, and Wind-Tunnel Testing of a Digital Controller System for Flutter Suppression," 4th NASA Workshop on Computational Control of Flexible Aerospace Systems, Williamsburg, VA, July 1990.

8 Newsom, J. R., Abel, I., and Dunn, H. J.: "Application of Two Design Methods for Active Flutter Suppression and Wind-Tunnel Test Results," NASA TP-1653, May 1980.

9 Harvey, C. A., Johnson, T. L., and Stein, G.: "Adaptive Control of Wing/Store Flutter", AFFDL-TR-79-3081, April 1979.

10 Adams, W. M. Jr., Tiffany, S. H., and Bardusch, R. E.: "Active Suppression of an 'Apparent Shock Induced Instability'," AIAA/ASME 28th Structures, Structural Dynamics and Materials Conference, Monterey, CA, April 1987.

11 Fletcher, R. and Powell, M. J. D.: "A Rapidly Convergent Descent Method for Minimization," Computer Journal, Vol. 6, 1963/64.

12 Schmidt, D. K. and Chen, T. K.: "Frequency Domain Synthesis of a Robust Flutter Control Law," Journal of Guidance and Control, Vol. 9, May-June 1986, pp. 346-351.

13 Srinathkumar, S. and Adams, W. M. Jr.: "Active Flutter Suppression Using Invariant Zeros / Eigensystem Assignment," Guidance, Navigation, and Control Conference, August 1989, AIAA 89-3610.

14 Mukhopadhyay, V.: "Digital Robust Control Law Synthesis Using Constrained Optimization," Journal of Guidance, Control, and Dynamics, Vol. 12, March-April 1989, pp. 175-181.

15 Mukhopadhyay, V. and Newsom, J. R.: "A Multiloop System Stability Margin Study Using Matrix Singular Values," Journal of Guidance, Control, and Dynamics, Vol. 7, September-October 1984, pp. 582-587.

16 Kwakernaak, H. and Sivan, R.: Linear Optimal Control Systems, Wiley Interscience, New York, 1972.

17 Moore, B. C.: "Principal Component Analysis in Linear Systems: Controllability, Observability, and Model Reduction," IEEE Transaction on Automatic Control, Vol. AC-26, February 1981.